PHYSICAL REVIEW A VOLUME 10, NUMBER 6 DECEMBER 1974

Correlations of excited electrons. The study of channels in hyperspherical coordinates*†

C. D. Lin‡
Department of Physics, University of Chicago, Chicago, Illinois 60637
(Received 11 July 1974)

According to early experiments and calculations, doubly excited states of helium are grouped into channels (Rydberg series and continua) with very different excitation and decay probability. Macek has identified channels by using hyperspherical coordinates [$R = (r_1^2 + r_2^2)^{1/2}$, $\tan\alpha = r_2/r_1$, $\Omega \equiv \{\alpha, \hat{r}_1, \hat{r}_2\}$] and solving the Schrödinger equation initially at fixed R; each eigenvalue $U_\mu(R)$ and eigenfunction $\Phi_\mu(R;\Omega)$ characterizes one channel and the approximate solution of the whole equation has the form $F_\mu(R)\Phi_\mu(R;\Omega)$. We study the electron correlations in each channel by obtaining explicit expressions for the $\Phi_\mu(R;\Omega)$, and extend the range of Macek's investigation to higher channels. Pairs of orbital quantum numbers (l_1,l_2) are found to be quasiconstants for each channel; channels with the same (l_1,l_2) and (L,S,π) differ mainly in the degree of excitation of the radial correlation. Channel functions $\Phi_\mu(R;\Omega)$ of ^1S, $^1P+$, and $^3P+$ channels have an antinode at or near $\alpha = 45°$, while those of ^3S, $^1P-$, and $^3P-$ channels have a node at or near $\alpha = 45°$. An antinode or a node appears to occur generally at or near $\alpha = 45°$. This location of nodes in the minus and ^3S channels is shown to be related to the weakness of coupling both among these channels and to plus channels with the same (L,S,π) symmetry. Examples for H^- are discussed. The interactions between channels with different (l_1,l_2) are important where their potential curves are nearly degenerate. Examples of the effect of this degeneracy in the spectra of alkaline-earth atoms are indicated.

I. INTRODUCTION

The spectrum of helium states with two excited electrons was first studied systematically by Madden and Codling with synchrotron radiation.[1] This work showed that levels with the same $^1P^0$ classification are grouped into different Rydberg series with very different excitation cross sections and autoionization widths. In the more familiar spectra of single excitation, each series and its adjoining continuum—which are jointly called a "channel"—are easily identified by the quantum numbers of an independent particle model. In the spectra of double excitation, attempts to classify channels by independent-particle angular-momentum quantum numbers have failed thus far, because of the dominant effect of correlations.

The early efforts toward a classification were reviewed by Fano.[2] By that time calculations of double excitation had shown that the existence of channels with given total angular momentum but with very different properties is not limited to the $^1P^0$ example of the initial experiment but is common to all cases that have been studied. These calculations predict energy levels and decay widths with accuracy comparable to that of experimental results and generally agree with one another. Unfortunately, however, the calculations fail to characterize the channels themselves and the grouping of levels into channels emerges from analysis of the results as accidental. Only one approach, by Macek,[3] yields a grouping of levels into channels by reducing the Schrödinger equation to a single variable form with alternative optical potentials. Different channels correspond to different potential wells and the channel properties are related to the well shape. However, the method was not developed sufficiently to reveal the physical nature of each channel or to test the approximations adequately.

Macek's method solves the two-electron Schrödinger equation in hyperspherical coordinates. In this coordinate system, the radial distances of the two electrons from the nucleus, r_1 and r_2, are replaced by a single radial coordinate $R = (r_1^2 + r_2^2)^{1/2}$ and by a pseudoangle $\alpha = \arctan(r_2/r_1)$; the other angular coordinates of the two electrons θ_1, ϕ_1, θ_2, ϕ_2 are treated as usual. By assuming quasiseparability of the total wave function ψ into $\psi(R,\Omega) = F_\mu(R)\Phi_\mu(R;\Omega)$, where Ω represents the five angles (including the pseudoangle α), Macek calculated $\Phi_\mu(R;\Omega)$ numerically for fixed values of R to obtain potential curves $U_\mu(R)$ for the motion along R. The numerical method used by Macek prevented him from studying the nature of each potential curve.

This paper introduces a different numerical method to calculate $\Phi_\mu(R;\Omega)$ and the potential curves. The method will permit us to distinguish the effects of angular correlations, radial correlations, and exchange in determining the properties of a given potential curve. The use of hyperspherical coordinates is particularly suitable for this study. In this coordinate system, the correlations are mapped onto two of the five angles only, while the coordinate R represents the size of the system

and the other three angles (i.e., Euler angles) specify the orientation of the system; their variations do not affect the relative distances of the electrons.

No previous work has related the properties of the channels to the type and strength of correlations beyond qualitative discussions. In their initial interpretation of the data of Madden and Codling, Cooper, Fano, and Prats[4] suggested that two channels found experimentally, which they called the plus and minus series, are characterized by in-step and out-of-step radial motions of the two electrons, respectively. The in-step motion allows the two electrons to penetrate simultaneously near the nucleus where both excitation and autoionization occur, while the out-of-step motion does not. This suggestion explained qualitatively the origin of the plus- and minus-series character of the two channels. Roughly speaking, the out-of-step motion of the minus series should have an extra node in the wave function in α. However, later work pointed out that there are three series for $^1P^0$ converging to the $n=2$ limit of He^+ instead of only the two series observed experimentally. Thus one cannot account for all three channels in terms of the in-step and out-of-step radial motion of the two electrons. The analysis of this paper will indicate that radial correlations are actually most important for distinguishing the plus and minus series, but angular correlations cannot be disregarded completely.

In fact, the type of electron correlation characteristic of each channel will depend on the size of the system; that is, on the coordinate R. In the limit of large R, one electron is separated from the residual ion core; here the correlation is mainly radial and causes the field acting on the outer electron to be screened by the other electron. In the opposite limit of small R, the correlations are mainly determined by the kinetic energy, inclusive of the effect of the Pauli exclusion principle. In the intermediate region, the kinetic energy, the electrostatic potential energy, and the effect of exchange are all important. The primary goal of this paper is to describe the change of correlations with increasing R for a number of channels. This will be done, as in Macek's work, with reference to a Born-Oppenheimer approximation for the total wave function $\psi \sim F_\mu(R)\Phi_\mu(R;\Omega)$, analogous to the approximation of the wave functions of diatomic molecules, in which case R indicates the internuclear distance. The change of correlations will be represented by the variation of the angular function $\Phi_\mu(R;\Omega)$ as the system expands from $R=0$ to the $R=\infty$ limit, much as the electronic wave function of a molecule evolves from the united atom to the separated atom limit.

It is not obvious that a Born-Oppenheimer approximation should be valid in atomic problems. In molecular physics, because of the small ratio of electron and nuclear masses, the nuclei are slow, thus permitting the electrons to adjust their motions adiabatically to changes in the nuclear positions. This favorable circumstance is absent in our atomic problem. Nevertheless, the approximation will be seen to have considerable validity, apparently because of the slow variation of Coulomb interaction strength as the system expands. In particular, at low total energies, the kinetic energy of the motion along R is small compared with the kinetic energies of the motion in Ω; also, the relative magnitude of kinetic- and potential-energy terms depends on R only linearly. Therefore, the angular wave function $\Phi_\mu(R;\Omega)$ can adjust adiabatically to changes of R. These considerations will be developed in subsequent sections.

Alternative approaches have been attempted with the aim of identifying the characteristics of correlations of doubly excited channels. In particular, Wulfman,[5] Alper and Sinanoğlu[6] and more recently Sinanoğlu and Herrick[7] have approached the problem, starting from a classification based on the SO(4) symmetry group of hydrogenic wave functions. The Hamiltonian expressed in terms of a basis constructed from that symmetry was found to be almost diagonal. Interesting results have thus been obtained, especially in the more recent work. Our work differs, in essence, in the choice of a basis frame for the analysis of correlations. The use of hyperspherical coordinates permits us to distinguish the various types of correlation effects and to follow their changes as the system expands.

The use of a hyperspherical coordinate system in the study of two electrons in a Coulomb field and of other three-body systems is far from new.[8] Previous use for heliumlike problems was to provide trial wave functions for variational calculations[9] and a series expansion form of the ground-state wave function of helium near the nucleus.[10] The harmonic functions on the five-dimensional spherical surface (hyperspherical harmonics) are described in Morse and Feshbach's text.[11] Recently, this approach has been generalized to an N-electron atomic system by Knirk,[12] with particular emphasis on the ground states.

For any N-electron atomic system, it should be possible to study the singly excited and doubly excited states using the methods of this paper and those of Knirk. In particular, in the system where two electrons move in the field of a closed-shell ion core, the problem is similar to our two-electron system except that the pure Coulomb field of the nucleus is replaced by a screened potential.

Here again, when the two outer electrons come close to each other, the short-range correlation effects can be studied as a purely two-electron problem. As mentioned above, this is because the short-range correlation effect is determined by the kinetic energies including the effect of the Pauli exclusion principle. By studying the kinetic-energy operator at small R, we can obtain information about the short-range correlation effects. An application of this method of analysis to the spectra of alkali-earth metals will be indicated in Sec. VI.

In this paper we study the effect of correlations and its connection to the characterization of channels in doubly excited states. Later papers will give calculations of potential curves and energies for several combinations of L, S, π for He and H^-. For H^- this is the first calculation of this type. For He we extend Macek's calculations to several additional symmetries; we will also discuss shortcomings of the Born-Oppenheimer expansion in this type of problem.

II. SQUARED GRAND ANGULAR-MOMENTUM OPERATOR Λ^2

In this section we formulate the two-electron problem in hyperspherical coordinates and discuss it qualitatively. The nonrelativistic Hamiltonian expressed in the coordinates of separate electrons and in atomic units is

$$H = -\tfrac{1}{2}\nabla_1^2 - \tfrac{1}{2}\nabla_2^2 - \frac{Z}{r_1} - \frac{Z}{r_2} + \frac{1}{r_{12}}. \tag{1}$$

In Eq. (1) Z is the charge of the nucleus, r_1 and r_2 the distances of the two electrons from the nucleus, and r_{12} the separation between the two electrons. Following Macek,[3] we express the Schrödinger equation in hyperspherical coordinates as

$$\left(\frac{d^2}{dR^2} - \frac{\Lambda^2+15/4}{R^2} + \frac{C}{R} + 2E\right)(R^{5/2}\Psi) = 0, \tag{2}$$

where Ψ is the total wave function of the system and the factor $R^{5/2}$ is introduced to eliminate the first-order derivative with respect to R. In Eq. (2) the potential energy is $-C/R$, where

$$C = R\left(\frac{2Z}{r_1} + \frac{2Z}{r_2} - \frac{2}{r_{12}}\right)$$
$$= \frac{2Z}{\cos\alpha} + \frac{2Z}{\sin\alpha} - \frac{2}{(1-\sin 2\alpha\cos\theta_{12})^{1/2}}, \tag{3}$$

$\alpha = \arctan(r_2/r_1)$ and θ_{12} is the angle between the two electrons subtended from the nucleus. The important operator Λ^2 is defined as

$$\Lambda^2 = -\frac{1}{\sin^2\alpha\cos^2\alpha}\frac{d}{d\alpha}\left(\sin^2\alpha\cos^2\alpha\frac{d}{d\alpha}\right) + \frac{\vec{l}_1^{\,2}}{\cos^2\alpha} + \frac{\vec{l}_2^{\,2}}{\sin^2\alpha} \tag{4}$$

in this coordinate system, where $\vec{l}_1^{\,2}$ and $\vec{l}_2^{\,2}$ are the squared orbital angular-momentum operators for the two electrons. Its properties will be discussed below.

Equation (2) is similar in structure to the Schrödinger equation for the radial wave function of a hydrogen atom, with d^2/dR^2 the kinetic-energy operator for the radial motion, $(\Lambda^2+15/4)/R^2$ the centrifugal potential energy, and C an effective nuclear charge. However, the potential energy $-C/R$ depends here on angular coordinates and does not commute with the operator Λ^2. Even for an N-electron atomic system, the nonrelativistic Schrödinger equation in hyperspherical coordinates has the same form as Eq. (2) except for different definitions of the operator Λ^2 and C. From Eq. (2) we notice that the relative magnitudes of the centrifugal potential energy $(\Lambda^2+15/4)/R^2$ and the electrostatic potential energy $-C/R$ scale linearly with R. This slow variation in relative magnitude of the two potential-energy terms is characteristic of Coulomb interactions.

The operator C in Eq. (3) depends only on the relative radial distances of the two electrons (measured by α) and on the angle θ_{12} between them. Figure 1 is a three-dimensional plot of $-C(\alpha, \theta_{12})$ for $Z=1$ on the plane (α, θ_{12}) in the range $0 \leq \alpha \leq \frac{1}{2}\pi$ and $0 \leq \theta_{12} \leq \pi$. This is a plot of the potential surface at $R=1$. In the limit $\alpha \approx 0$ (or $\approx \frac{1}{2}\pi$), the potential surface has a sharp drop caused by the electron-nucleus attraction. In the situations where $r_1 \approx r_2$, which corresponds to $\alpha \approx \frac{1}{4}\pi$, the potential energy depends critically on whether θ_{12} approximates π or zero. When $\theta_{12} \approx 0$, $\alpha = \frac{1}{4}\pi$, the two electrons lie close to each other in the configuration space where a large electron-electron repulsion is expected. In Fig. 1 this repulsion appears as a spike near $\theta_{12}=0$ and $\alpha = \frac{1}{4}\pi$. Over a large area around the saddle point at $(\alpha = \frac{1}{4}\pi, \theta_{12} = \pi)$ the potential surface is very flat. Our task is to study the pattern of standing waves on this potential surface.

The operator Λ^2 has been studied in the context of three-body collisions by Smith[13] and is the square of the grand angular-momentum operator $\vec{\Lambda}$. It is a straightforward generalization of the squared angular-momentum operator from three to six dimensions and is thus the Casimir operator for the group O(6). Its eigenvalues are $\nu(\nu+4)$, with ν a non-negative integer. In ordinary three-dimensional space, the eigenvalues of the angular-momentum operator measure the strength of the centrifugal field which pushes the particle away from a force center. Similarly, the quantum number ν indicates the strength of the field that keeps a pair of particles from approaching a force center simultaneously. The operator Λ^2 commutes

with L^2, S^2, and π, where L^2, S^2 are the total orbital and spin squared angular momenta of the system, respectively, and π is the parity. Therefore, its eigenvalue would be a constant of motion in the absence of a force field, such as $-C/R$, which depends on angular variables. Furthermore, Λ^2 also commutes with operators of subgroups of O(6); for example, it commutes with the squared angular-momentum operators for each of the two electrons, $\vec{l}_1^2$ and $\vec{l}_2^2$, whose eigenvalues are $l_1(l_1+1)$ and $l_2(l_2+1)$. This implies a degeneracy of its eigenvalues. Since Λ^2 doesn't commute with C, the degeneracy is removed in the presence of this potential field and ν is no longer a good quantum number.

Since the electron-nucleus interaction component within C commutes with $\vec{l}_1^2$ and $\vec{l}_2^2$ and thus preserves the quantum numbers l_1 and l_2 of the two electrons, the hyperspherical coordinates we have chosen will prove suitable for describing the dynamics of two electrons in a Coulomb field. In this particular representation the operator Λ^2 has the form given by Eq. (4) and its eigenfunctions $v_{l_1l_2m}(\Omega)$ are labeled with quantum numbers l_1 and l_2 and m, where m is a non-negative integer, related to ν by $\nu = l_1 + l_2 + 2m$. The first-order derivative term $d/d\alpha$ in the eigenvalue equation $[\Lambda^2 - \nu(\nu+4)]v_{l_1l_2m}(\Omega) = 0$ can be eliminated by introducing $u_{l_1l_2m}(\alpha, \hat{r}_1, \hat{r}_2) = \sin\alpha\cos\alpha v_{l_1l_2m}(\alpha, \hat{r}_1, \hat{r}_2)$, where $u_{l_1l_2m}(\Omega)$ satisfies

$$\left(-\frac{d^2}{d\alpha^2} + \frac{\vec{l}_1^2}{\cos^2\alpha} + \frac{\vec{l}_2^2}{\sin^2\alpha} - (\nu+2)^2\right)u_{l_1l_2m}(\Omega) = 0 . \tag{5}$$

The eigenfunctions $u^{SLM}_{l_1l_2m}(\Omega)$, with symmetry $(-1)^S$ for singlet or triplet states with fixed L, M, S, π are given by[14]

$$u^{SLM}_{l_1l_2m}(\Omega) = \frac{1}{\sqrt{2}}\left[f_{l_1l_2m}(\alpha)\mathcal{Y}_{l_1l_2LM}(\hat{r}_1, \hat{r}_2) + (-1)^{l_1+l_2-L+S+m} f_{l_2l_1m}(\alpha)\mathcal{Y}_{l_2l_1LM}(\hat{r}_1, \hat{r}_2)\right] \text{ if } l_1 \neq l_2$$

$$= \tfrac{1}{2}\left[1 + (-1)^{-L+S+m}\right] f_{llm}(\alpha)\mathcal{Y}_{llLM}(\hat{r}_1, \hat{r}_2) \text{ if } l_1 = l_2 = l . \tag{6}$$

In Eq. (6), Ω represents the five angles α, θ_1, ϕ_1, θ_2, ϕ_2 and $\hat{r}_1 \equiv (\theta_1, \phi_1)$, $\hat{r}_2 \equiv (\theta_2, \phi_2)$. The function $\mathcal{Y}_{l_1l_2LM}(\hat{r}_1, \hat{r}_2)$, given in Eq. (9) of Ref. 14, is the total orbital angular-momentum eigenfunction constructed from the orbital angular-momentum eigenfunctions of the two electrons; here the quantum number pair (l_1l_2) is ordered. The function $f_{l_1l_2m}(\alpha)$ is defined as

$$f_{l_1l_2m}(\alpha) = N_{l_1l_2m}(\cos\alpha)^{l_1+1}(\sin\alpha)^{l_2+1} \times F(-m, m+l_1+l_2+2 \,|\, l_2+\tfrac{3}{2} \,|\, \sin^2\alpha) , \tag{7}$$

where $N_{l_1l_2m}$ is a normalization constant given explicitly in Ref. 14. The quantum number pair (l_1l_2) is also ordered in $N_{l_1l_2m}$ and $f_{l_1l_2m}$. By contrast, it is not ordered in the symmetrized basis functions $u^{SLM}_{l_1l_2m}(\Omega)$, in which case we set $l_1 \geq l_2$. In Eq. (7) $F(-m, m+l_1+l_2+2 \,|\, l_2+\frac{3}{2} \,|\, \sin^2\alpha)$ is proportional to a Jacobi polynomials of degree m in $\sin^2\alpha$, with m nodes in the range $0 < \alpha < \frac{1}{2}\pi$. Since we are always discussing states with fixed L, S, π, these indices will be usually dropped.

For a given state, the angular correlation is represented by the statistical distribution of the wave function in the range $0 \leq \theta_{12} \leq \pi$. Our basis function $u_{l_1l_2m}(\Omega)$ is not expressed as a function of θ_{12} explicitly. However, we can expand $\mathcal{Y}_{l_1l_2LM} \times(\hat{r}_1, \hat{r}_2)$ and $\mathcal{Y}_{l_2l_1LM}(\hat{r}_1, \hat{r}_2)$ in Eq. (6) in terms of Legendre polynomials $P_k(\cos\theta_{12})$ of degree k. For $L=0, M=0$, we have

$$u_{l_1l_2m}(\Omega) = (-1)^l \frac{(2l+1)^{1/2}}{4\pi} P_l(\cos\theta_{12}) f_{llm}(\alpha) \times \tfrac{1}{2}\left[1 + (-1)^{L+S+m}\right], \tag{8}$$

and for $L=1$, $M=0$, $\pi=-1$, and $l_2 = l_1 - 1$

$$u_{l_1l_2m}(\Omega) = \frac{1}{4\sqrt{2\pi}\, l_2}\left[\left[Y_{10}(\hat{r}_1) + Y_{10}(\hat{r}_2)\right]\left[f_{l_1l_2m} + (-1)^{S+m} f_{l_2l_1m}\right]\left(\sum_{k=0}^{l_2}(-1)^k(2k+1)P_k(\cos\theta_{12})\right) + \left[Y_{10}(\hat{r}_1) - Y_{10}(\hat{r}_2)\right] \times \left[f_{l_1l_2m} - (-1)^{S+m} f_{l_2l_1m}\right]\left(\sum_{k=0}^{l_2}(2k+1)P_k(\cos\theta_{12})\right)\right] , \tag{9}$$

where $Y_{L0}(\hat{r}_i) = [(2L+1)/4\pi]^{1/2} P_L(\cos\theta_i)$. The basis functions of Eq. (8) are products of a function of θ_{12} and of a function of α only. For $L \neq 0$, one cannot separate the two angles α and θ_{12}. In Eq. (9), the first term is peaked near $\theta_{12} = \pi$ and the second term is peaked near $\theta_{12} = 0$, the more sharply the larger $l_2 = l_1 - 1$.

In Eq. (2), the potential energy $-C/R$ depends explicitly on θ_{12}. It might then seem natural to choose θ_{12} as one of the angular coordinates.[15]

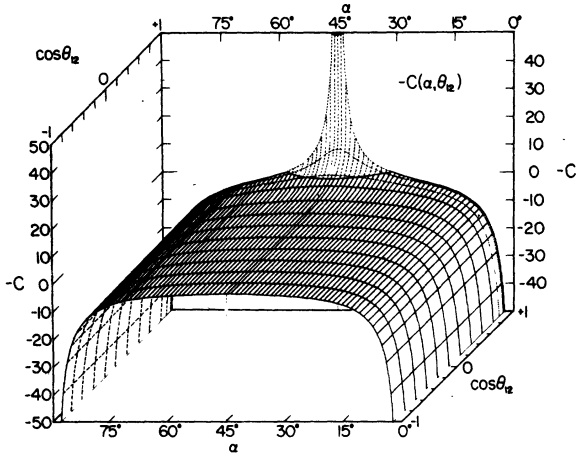

FIG. 1. Three-dimension plot of $-C(\alpha,\theta_{12})$ with $Z=1$ in hyperspherical coordinates; the ordinates represent a potential surface in Rydberg units at $R=1$ bohr (courtesy of C. E. Theodosiou).

However, we prefer to use $(\theta_1, \phi_1, \theta_2, \phi_2)$ as angular coordinates because of other advantages. First, in the dissociation limit ($\alpha \approx 0$) in which one electron is moving far away from the rest of the system, these coordinates reduce smoothly to independent-particle coordinates. By taking the limit $\alpha \to 0$ and $R \to \infty$ such that $r_2 = R\sin\alpha$ remains finite and $r_1 = R\cos\alpha \approx R$, Eq. (2) can be easily transformed to the sum of two hydrogenlike Schrödinger equations in the coordinate (r_2, θ_2, ϕ_2) and (r_1, θ_1, ϕ_1), respectively, with charges Z and $Z-1$. At this limit, the angular correlation between the two electrons is unimportant; use of θ_{12} would require a frame transformation in this limit. Second, using $(\theta_1, \phi_1, \theta_2, \phi_2)$, we can label the eigenfunctions of Λ^2 by l_1 and l_2. These quantum numbers will prove useful in that the matrix elements of C are almost diagonal with respect to the pair (l_1, l_2). Third, the symmetrization or antisymmetrization of the basis function is very simple in this coordinate system but nontrivial if θ_{12} is used.[16]

Using the basis set $\{u_{l_1 l_2 m}\}$ for the expansion $R^{5/2}\sin\alpha\cos\alpha\Psi = \sum_{l_1 l_2 m} g_{l_1 l_2 m}(R) u_{l_1 l_2 m}(\Omega)$, the Schrödinger equation (2) reduces to an infinite set of coupled differential equations, written in matrix form as

$$\left[\left(\frac{d^2}{dR^2} + \frac{1/4}{R^2} - \frac{(l_1+l_2+2m+2)^2}{R^2} + 2E\right)\underline{I} + \underline{C}/R\right]\vec{g}(R) = 0, \tag{10}$$

where $\underline{I}$ is the identity matrix and $-\underline{C}/R$ is the Coulomb interaction matrix, both of infinite dimensions, and $\vec{g}(R)$ is a column vector. The properties of this set of coupled differential equations at small R have been studied recently by Macek[14] and by Knirk.[12] The evaluation of the matrix elements of C, $(l_1' l_2' m' | C | l_1 l_2 m)$ has required considerable effort in the present work. A detailed derivation and the resulting formulas for computer calculations are given elsewhere.[17]

In Table I, we give some of the matrix elements $(l_1' l_2' m' | C | l_1 l_2 m)$ calculated for ^1S states and $Z=2$. In this particular example, m is limited to even values. From the table, which is quite representative of other cases, we observe the following.

(a) The diagonal matrix elements $(l_1 l_2 m | C | l_1 l_2 m)$ are always much larger than the off-diagonal ones. Also, $(l_1 l_2 m | C | l_1 l_2 m)$ decreases with increasing $l_1 + l_2$ and constant m, but it increases with increasing m at constant (l_1, l_2).

(b) The matrix elements diagonal in the (l_1, l_2) pair are much larger than the off-diagonal ones, because the electron-nucleus interactions are diagonal in (l_1, l_2). In addition, in the electron-electron interaction matrix elements, the integrals over α are largest for the monopole component, i.e., for

TABLE I. Matrix elements $(l_1 l_2 m | C | l_1' l_2' m')$ for helium ^1S states.

$(l_1' l_2' m')$ \ $(l_1 l_2 m)$	$(\nu+2)^2$	(000) 4	(002) 36	(004) 100	(006) 196	(110) 16	(112) 64	(114) 144	(220) 36	(222) 100	(330) 64
(000)		11.18	3.70	1.99	1.50	0.96	−0.20	0.09	−0.58	0.17	0.41
(002)			16.86	7.18	4.60	−0.47	0.65	−0.16	0.39	−0.33	−0.32
(004)				19.48	9.24	0.15	−0.46	0.59	−0.20	0.33	0.20
(006)					21.19	−0.08	0.13	−0.47	0.10	−0.19	−0.12
(110)						9.40	2.12	0.51	1.34	−0.36	−0.88
(112)							13.06	4.06	−0.59	0.85	0.51
(114)								15.10	0.25	−0.55	−0.29
(220)									8.80	1.61	1.52
(222)										11.66	−0.62
(330)											8.47

the component that does not involve any angular momentum transfer between two electrons. Physically this means that the screening effect—which has central symmetry—includes most of the electron-electron interaction. This contribution to $-C/R$ is diagonal in (l_1, l_2).

III. PROBLEM OF IDENTIFYING CHANNELS

From the discussion of Sec. I, we know that doubly excited states are grouped into channels. The infinite set of coupled equations [(10)] doesn't display the channel characters because the off-diagonal terms of its matrix C become increasingly important as R increases. The empirical fact that the channels are weakly coupled implies that the channels are best specified if the coupling terms in the system of differential equations can be minimized. Macek has used the *Ansatz* $\psi_\mu^i(R, \Omega) = F_\mu^i(R)\Phi_\mu(R; \Omega)$, for which all the doubly excited states i within a given channel μ have the same angular wave function $\Phi_\mu(R; \Omega)$. This approximation implies that the coupling terms can be neglected and that each channel is characterized by the different type and strength of correlations represented by the wave function $\Phi_\mu(R; \Omega)$.

The physical argument for separating R from the five angular coordinates in the identification of channels is discussed elsewhere.[18] In this section we shall study the mathematical definition of channels. Beginning from the complete set of coupled differential equations [(10)], we study its transformation from the representation in the basis of $u_{l_1 l_2 m}(\Omega)$ to other bases for which the magnitude of the coupling terms is reduced.

Equation (10) is almost diagonal at small R; therefore, each channel is characterized by the quantum numbers $(l_1 l_2 m)$ at small R. The wave function $\Phi_\mu(R; \Omega)$ for each channel at small R coincides then with $u_{l_1 l_2 m}(\Omega)$. As R increases, the off-diagonal terms in $-C/R$ become increasingly important. To minimize the coupling at each R, we make a suitable transformation of the basis $\{u_{l_1 l_2 m}(\Omega)\}$ to a new basis $\{\Phi_\mu(R; \Omega)\}$ in which the complete wave function is expanded as

$$\psi(R; \Omega) = \sum_\mu F_\mu(R)\Phi_\mu(R; \Omega) . \tag{11}$$

The system of coupled differential equations for the $F_\mu(R)$ is then

$$\left[\left(\frac{d^2}{dR^2} + \frac{1/4}{R^2} + 2E\right)\underline{I} - \underline{U}(R) + \underline{W}(R)\right]\vec{F}(R) = 0 \tag{12}$$

where $\underline{I}$ is the identity matrix,

$$U_{\mu,\nu}(R) = \frac{1}{R^2}\left(\Phi_\mu(R; \Omega)\left| -\frac{d^2}{d\alpha^2} + \frac{\vec{l}_1^2}{\cos^2\alpha} + \frac{\vec{l}_2^2}{\sin^2\alpha} - RC\right|\Phi_\nu(R; \Omega)\right) , \tag{13}$$

and

$$W_{\mu,\nu}(R) = 2\left(\Phi_\mu(R; \Omega), \frac{d}{dR}\Phi_\nu(R; \Omega)\right)\frac{d}{dR} + \left(\Phi_\mu(R; \Omega), \frac{d^2}{dR^2}\Phi_\nu(R; \Omega)\right) . \tag{14}$$

In Eqs. (13) and (14) the parentheses mean integration over the set of angles represented by Ω. Our purpose is to choose Φ_μ such that the off-diagonal matrix elements of $\underline{U}$ and $\underline{W}$ are as small as possible.

The matrix $\underline{W}(R)$ which appears in Eq. (12) but is absent in Eq. (10) comes from the R dependence of $\Phi_\mu(R; \Omega)$. Its off-diagonal elements contribute to the coupling between channels together with those of the matrix $\underline{U}$. Since the two matrices $\underline{U}$ and $\underline{W}$ do not commute, one cannot diagonalize them simultaneously so as to cancel the coupling terms altogether. Qualitatively, the observation that channels are weakly coupled implies the existence of basis functions $\Phi_\mu(R, \Omega)$ for which the off-diagonal terms of $\underline{U} - \underline{W}$ are small at all R. Since the matrix $\underline{W}$ contains nonlocal operator d/dR, it is not clear how to define a minimization condition for the coupling terms. Therefore, we approach the problem of minimization empirically.

Equations (11) and (12) are analogous to equations of the so-called molecular-wave-function expansion in molecular physics, in which case R is the internuclear distance of two atoms, $F_\mu(R)$ is a nuclear wave function and $\Phi_\mu(R; \Omega)$ an electronic wave function. Molecular physics considers two familiar representations of $\Phi_\mu(R; \Omega)$: the adiabatic representation in which $\underline{U}$ is diagonal and the diabatic representation in which $\underline{W}$ is diagonal.[19] In the adiabatic representation, one obtains the Born-Oppenheimer approximation by disregarding the off-diagonal elements of $\underline{W}$. This approximation was used by Macek in our problem to obtain adiabatic potential curves which are plots of the diagonal terms of $\underline{U}$. In this representation the off-diagonal terms of $\underline{W}$ may be large, especially in ranges of R where two adiabatic potential curves are nearly degenerate. Transformation to an alternative representation, e.g., a diabatic one, may then serve to reduce the magnitude of the off-diagonal terms of $\underline{W}$ without increasing those of $\underline{U}$ ex-

cessively.

It must be emphasized that there are no formal restrictions on the choice of the functions $\Phi_\mu(R;\Omega)$ except that they form a complete basis set at each R. Equation (12) contains no approximations if the full matrices $\underline{U}$ and $\underline{W}$ are retained, independently of the representation which is chosen. In fact, one can choose representations in which neither $\underline{U}$ nor $\underline{W}$ is diagonal. The transformation properties of $\underline{U}$ and $\underline{W}$ from one representation to another have been studied by Smith in Ref. 19 and are summarized in Ref. 17.

We take advantage of the flexibility in the choice of $\Phi_\mu(R;\Omega)$ to unravel the electron correlations. To this end, we shall not use either an adiabatic or a diabatic representation in the first step of calculations but choose angular wave functions

$$\phi_\rho^{(l_1l_2)}(R;\Omega)=\sum_m u_{l_1l_2m}(\Omega)a_m^\rho(l_1l_2,R), \tag{15}$$

which diagonalize only the submatrix of $\underline{U}$ in each subspace with fixed (l_1l_2). This is done by diagonalizing at each value of R submatrices of the form

$$(l_1l_2m|U|l_1l_2m')=\frac{(l_1+l_2+2m+2)^2}{R^2}\delta_{mm'}-\frac{(l_1l_2m|C|l_1l_2m')}{R}, \tag{16}$$

where the integers m and m' run from 0 to ∞. In this representation with basis functions $\phi_\rho^{(l_1l_2)}$, the complete matrices of $\underline{U}$ and $\underline{W}$ have the form

$$(l_1l_2\rho'|U(R)|l_1l_2\rho)=v_\rho^{(l_1l_2)}(R)\delta_{\rho\rho'}, \tag{17a}$$

$$(l_1'l_2'\rho'|U(R)|l_1l_2\rho)=-(l_1'l_2'\rho'|C|l_1l_2\rho)/R \quad \text{when } (l_1'l_2')\neq(l_1l_2), \tag{17b}$$

$$(l_1'l_2'\rho'|W(R)|l_1l_2\rho)=(l_1l_2\rho'|W(R)|l_1l_2\rho)\delta_{l_1l_1'}\delta_{l_2l_2'}. \tag{17c}$$

Each channel $(l_1l_2\rho)$, defined mathematically above, is characterized by the channel function $\phi_\rho^{(l_1l_2)}(R;\Omega)$ and by the optical potential $v_\rho^{(l_1l_2)}(R)$. In this basis set $\{\phi_\rho^{(l_1l_2)}(R;\Omega)\}$, neither $\underline{U}$ nor $\underline{W}$ is diagonal. However, $\underline{U}$ has off-diagonal terms between channels of different (l_1l_2) pairs only, whereas $\underline{W}$ has off-diagonal terms between channels with the same (l_1l_2) only. The off-diagonal term of $\underline{U}$, given in Eq. (17b), is of the order $(l_1'l_2'm'|C|l_1l_2m)/R$, where $(l_1'l_2'm'|C|l_1l_2m)$ is rather small, as indicated in Sec. II. Therefore, even though $\underline{U}$ is not diagonal in this representation, its nondiagonal terms are important only when their magnitudes are comparable with the differences of the corresponding diagonal terms.

The representation we have chosen is suitable for unraveling electron correlations because, in each (l_1l_2) subspace, different channel functions $\phi_\rho^{(l_1l_2)}$ correspond to different patterns of radial correlation. These patterns will be described in Sec. IV together with the angular correlations that result only from the coupling of angular momenta. The alternative patterns of correlation, both radial and angular, represented by the various channel functions $\phi_\rho^{(l_1l_2)}$ are, however, superposed by the action of the matrix elements (17b) which causes transfer of orbital momentum between two electrons and mix the channels of different (l_1l_2) subspaces. This superposition results from a second step of transformation to a new basis set, $\{\Phi_\mu(R;\Omega)\}$. As developed in Sec. V, this second step will have the effect of diagonalizing the matrix $\underline{U}$, thus reproducing and extending Macek's results. However, we would like to emphasize that diagonalization of $\underline{U}$ is not necessarily a desired goal. In order to establish the closest correspondence with the physically observed channels, one should find a representation $\Phi_\mu(R;\Omega)$ in which the off-diagonal terms of $\underline{U}$ and $\underline{W}$ are *minimized simultaneously*, though neither matrix is diagonal.

IV. DESCRIPTIONS OF CHANNELS $\phi_\rho^{(l_1l_2)}$ WITHIN FIXED (l_1l_2)

In this section we will describe the properties of the potential curves and of channel functions $\phi_\rho^{(l_1l_2)}\times(R;\Omega)$ for various sample channels $(l_1l_2\rho)$ within subspaces of fixed (l_1l_2), obtained by the method described in Sec. III. Since all of the discussions in this section are within a fixed (l_1l_2) subspace, the superscripts in $v_\rho^{(l_1l_2)}$ and $\phi_\rho^{(l_1l_2)}$ may be dropped. In Sec. IV A we examine $v_\rho(R)$ and the properties of $\phi_\rho(R;\Omega)$ in the limits of $R\to 0$ and $R\to\infty$. The coordination scheme, i.e., the rule of evolution of the potential curves $v_\rho(R)$ and the properties of channel functions $\phi_\rho(R;\Omega)$ at intermediate R, are discussed in Sec. IV B for the special case $l_1=l_2$. (This class includes not only all S states but also others, i.e., $p^2\,{}^3P$ and $p^2\,{}^1D$.) The variations of $\phi_\rho(R;\Omega)$ with R for a given channel ρ and the difference in the properties of $\phi_\rho(R;\Omega)$ between different channels ρ will be examined in detail. In Sec. IV C the general case of $l_1\neq l_2$ is discussed with particular reference to P^0 states. We will show that the pair of channels with the plus and minus character mentioned in the Introduction occur quite generally. In Sec. IV D the coupling terms in W, i.e., $(l_1l_2\rho|W|l_1l_2\rho')$, are discussed with reference to the excitation mechanism.

A. Limits $R \to 0$ and $R \to \infty$

1. $R \to \infty$ *limit*

At small R, the off-diagonal terms $(l_1 l_2 m | C | l_1 l_2 m')/R$ in Eq. (16) are much smaller than $[(l_1 + l_2 + 2m + 2)^2 - (l_1 + l_2 + 2m' + 2)^2]/R^2$ and therefore can be disregarded. From Eq. (16), $v_\rho(R)$ is given by

$$v_\rho(R) \to [(l_1 + l_2 + 2m + 2)^2 - R(l_1 l_2 m | C | l_1 l_2 m)]/R^2 \text{ as } R \to 0 . \quad (18)$$

Since (l_1, l_2) is fixed, the potential curves $v_\rho(R)$ at small R are ordered with increasing m without degeneracy, and each channel function $\phi_\rho(R; \Omega)$ is approximated by the basis function $u_{l_1 l_2 m}(\Omega)$. The properties of each channel ρ at small R are therefore determined by the properties of $u_{l_1 l_2 m}(\Omega)$ for different m.

The function $u_{l_1 l_2 m}(\Omega)$, as given in Eq. (6), is a five-variable nonseparable function. However, for $L = 0$, we have $l_1 = l_2 = l$ and u_{llm} reduces to the product of a function $f_{llm}(\alpha)$ of α and of a function of θ_{12}, as shown by Eq. (8). In other words, the channel function in this limit *can be separated* into a function of α that represents the *radial correlation* and a function of θ_{12} that represents the *angular correlation*; this function is independent of the orientation in space of the vector $(\hat{r}_1, \hat{r}_2)$ since it pertains to an S state. With l fixed in each subspace, the function of θ_{12} is the same for all channels and different channel functions differ only in their α-dependent part for various m; the angular correlations, represented by a function of θ_{12}, depend on l. For fixed l, channels with increasing ρ correspond to increasing degrees of excitation of radial correlations; as usual, excitation to a higher harmonic $\phi_\rho(R; \Omega) \sim f_{llm}(\alpha)$ requires higher-energy v_ρ. The effect of Pauli exclusion principle is, in this case, to restrict the quantum number m to even values for singlets or odd values for triplets. Thus, in this simple case, the effect of radial correlation can be separated from the effect of angular correlation and of exchange, at least in the limit of $R \to 0$.

When $l_1 \neq l_2$, the function $u_{l_1 l_2 m}(\Omega)$ is no longer quite factorable into functions of α and of $(\hat{r}_1, \hat{r}_2)$. Therefore, the radial correlations are not completely independent of angular and exchange correlations. As given in Eq. (6), the symmetrized function $u_{l_1 l_2 m}(\Omega)$ is the sum of two product functions, superposed according to the symmetrization condition required by the Pauli principle. In each of two product functions—$f_{l_1 l_2 m}(\alpha) \mathcal{Y}_{l_1 l_2 L M}(\hat{r}_1, \hat{r}_2)$ and $f_{l_2 l_1 m}(\alpha) \mathcal{Y}_{l_2 l_1 L M}(\hat{r}_1, \hat{r}_2)$—the α-dependent part separates from the $(\hat{r}_1, \hat{r}_2)$-dependent part; i.e., the part that represents radial correlation separates from the part that represents angular correlations. Exchange superposes these two product functions, thus generating a more complicated pattern of correlations. Different functions $u_{l_1 l_2 m}$ of the same $(l_1 l_2)$ spaces differ, however, only in their degree of radial correlation represented by the function $f_{l_1 l_2 m}(\alpha)$.

2. $R \to \infty$ *limit*

In this limit, one electron is moving far outside the ionic core. The channel function $\phi_\rho(R; \Omega)$ is concentrated at small α in the deep well of the potential surface of Fig. 1 (or in the symmetric well at $\alpha \sim \frac{1}{2}\pi$). Physically, in this limit, the two-electron wave function is represented by the product of two hydrogenic wave functions, one with the full charge Z, the other with screened charge $(Z - 1)$. One can expand $\phi_\rho(R; \Omega)$ near $\alpha \to 0$ and $R \to \infty$ as done in Ref. 3, but we choose to transform the operator U of Eq. (13) back into independent-particle coordinates $r_1 = R \cos\alpha \approx R$, $r_2 = R \sin\alpha$, and then expand the transformed equation in powers of $1/R$; we obtain[17]

$$U\phi_\rho = \left[-\left(\frac{d^2}{dr_2^2} - \frac{\vec{l}_2^{\,2}}{r_2^2} + \frac{2Z}{r_2} \right) - \frac{2(Z-1)}{R} + \frac{1}{R^2} \left(r_2^2 \frac{\partial^2}{\partial r_2^2} + r_2 \frac{\partial}{\partial r_2} + \vec{l}_1^{\,2} + 2 r_2 \cos\theta_{12} \right) + O\left(\frac{1}{R^3} \right) \right] \phi_\rho(\vec{r}_1, \vec{r}_2) = v_\rho(R) \phi_\rho(\vec{r}_1, \vec{r}_2) , \quad (19)$$

where R is treated as a parameter. This equation is similar to Eq. (15) of Ref. 3. The difference in the $1/R^2$ terms comes from the fact that we have set $r_2 = R \sin\alpha$ instead of expanding in the form $r_2 \approx R\alpha$. In Eq. (19), the orbital quantum number in the first parentheses can take alternative values of (l_1, l_2). At large R we take ϕ_ρ to be an eigenfunction of the operator in the first parentheses in Eq. (19) and evaluate v_ρ by perturbation theory. For $l_1 = l_2 = l$ we get

$$\phi_\rho = P_{nl}(r_2) \mathcal{Y}_{llLM}(\hat{r}_1, \hat{r}_2) , \quad (20a)$$

where $P_{nl}(r_2)$ is a radial hydrogenic wave function. The $1/R^2$ terms of v_ρ are then obtained by evaluating $(\phi_\rho | r_2^2 \partial^2/\partial r_2^2 + r_2 \partial/\partial r_2 + \vec{l}_1^{\,2} + 2 r_2 \cos\theta_{12} | \phi_\rho)$. As shown in Ref. 17, the derivative terms in this expression are cancelled by $-[\frac{1}{4}/R^2 + W_{\rho,\rho}(R)]$. Therefore, we obtain

$$[v_\rho(R) - \tfrac{1}{4}/R^2 - W_{\rho,\rho}(R)] \to -\frac{Z^2}{n^2} - \frac{2(Z-1)}{R} + \frac{1}{R^2} (\phi_\rho | \vec{l}_1^{\,2} + 2 r_2 \cos\theta_{12} | \phi_\rho) \text{ as } R \to \infty , \quad (20b)$$

where n is the principal quantum number. Thus, in the large-R limit, the potential curves are ordered with increasing n in each (ll) subspace and the channel functions are represented by $P_{nl}(r_2) \times \mathcal{Y}_{llLM}(\hat{r}_1, \hat{r}_2)$. For $l_1 \neq l_2$, two channel potentials converge to each hydrogenic limit n and are degenerate. In this case, ϕ_ρ is a superposition of $P_{nl_2}(r_2)\mathcal{Y}_{l_1l_2LM}(\hat{r}_1, \hat{r}_2)$ and $P_{nl_1}(r_2)\mathcal{Y}_{l_2l_1LM}(\hat{r}_1, \hat{r}_2)$ controlled by the dipole interaction $2r_2\cos\theta_{12}/R^2$ of Eq. (19).

It should be noted that the hydrogenic limit terms of the energy eigenvalue (20b), namely, $-Z^2/n^2 - 2(Z-1)/R$, are independent of (l_1, l_2). Therefore channel potentials of different (l_1, l_2) subspaces converge in general to the same limit at $R \to \infty$, thus increasing the quasidegeneracy of channel potentials at large R. The dipole interaction in the last term of (20b) couples all these channels, whether in the same or in different (l_1, l_2) subspaces. Separate analysis of the channels in (l_1, l_2) subspaces thus loses interest in the large-R limit.

B. Coordination scheme of $\nu_\rho^{(l_1l_2)}$ and properties of $\phi_\rho^{(l_1l_2)}(R;\Omega)$ with $l_1 = l_2$

We proceed now to study the evaluation of $\upsilon_\rho^{(l_1l_2)}(R)$ and the properties of $\phi_\rho^{(l_1l_2)}(R;\Omega)$ in the special case $l_1 = l_2 = l$. Figure 2(a) shows the lowest three potential curves $\upsilon_\rho(R)$ for the doubly excited helium ^1S states with $(l_1, l_2) = (0, 0)$, each converging to a different n limit of He^+. The $\rho = 0$ curve converges to $n = 1$ limit of He^+ and thus represents single excitation; it is shown on a different energy scale. Remarkably, these curves remain close to their limiting values, Eqs. (18) and (20b), over a wide range of R. The low-R behavior is displayed better by plotting $R^2\upsilon_\rho(R)$, as shown in Fig. 2(b). Here $R^2\upsilon_\rho(R)$ has a large region of linear dependence on R before turning into the quadratic dependence characteristic of the large-R limit. The region of transition from linear to quadratic dependence is characterized by avoided crossings between neighboring curves.

For comparison, in Fig. 2(c) we plot the lowest four curves of $R^2\upsilon_\rho(R)$ for helium ^3S states with $(l_1, l_2) = (0, 0)$. A striking difference of these plots from those of Fig. 2(b) is that these curves change from the region of linear dependence on R into the region of quadratic dependence without any region of avoided crossings; i.e., these curves behave independently and hardly repel each other, in contrast to the curves of Fig. 2(b). As we will see below, this difference appears to reflect a fundamental difference in the properties of excitation mechanism.

The curves shown in Figs. 2(b) and 2(c) never approach each other. Thus they not only follow the noncrossing rule, but do not even show any sharp avoided crossing. Accordingly, the channel functions $\phi_\rho(R;\Omega)$ should vary slowly with R. For $l_1 = l_2 = l$, each channel function can be expressed as

$$\phi_\rho = \sum_m a_m^\rho(R)\boldsymbol{u}_{llm}(\Omega) = \left(\sum_m a_m^\rho(R) f_{llm}(\alpha)\right)\mathcal{Y}_{llLM}(\hat{r}_1, \hat{r}_2)$$

$$\equiv g_\rho(R;\alpha)\mathcal{Y}_{llLM}(\hat{r}_1, \hat{r}_2), \qquad (21)$$

thus factoring into separate functions of α and of $(\hat{r}_1, \hat{r}_2)$, as it does in the $R \to 0$ and $R \to \infty$ limits. In fact, in both limits, ρ equals the number of nodes in the range $0 < \alpha < \frac{1}{4}\pi$. Similarly, in the intermediate region, functions $g_\rho(R;\alpha)$ with increasing ρ have an increasing number of nodes and thus represent increasing excitation of radial correlation. Therefore, ρ can serve as a good meaningful quantum number over the whole range of R. The variation of $g_\rho(R;\alpha)$ with increasing R shifts the distribution of nodes progressively away from the midpoint $\alpha = \frac{1}{4}\pi$. In Figs. 3(a) and 3(b), we plot $g_\rho(R;\alpha)$ for several values of increasing R in the range $0 < \alpha < \frac{1}{4}\pi$ for the $\rho = 1$ curves of Figs. 2(b) and 2(c), respectively; the range $\frac{1}{4}\pi < \alpha < \frac{1}{2}\pi$ is not shown because $g_\rho(R;\alpha)$ is symmetric for singlets and antisymmetric for triplets with respect to reflection at $\alpha = \frac{1}{4}\pi$. For both figures we can consider the behavior of $g_\rho(R;\alpha)$ in two distinguishable regions: (A), where $R^2\upsilon_\rho(R)$ varies linearly with R, and (B), where $R^2\upsilon_\rho(R)$ varies quadratically with R. In region (A), $\upsilon_\rho(R)$ is much larger than the potential energy $-C(\alpha, \theta_{12})/R$ in the flat region of Fig. 1. Therefore, $g_\rho(R;\alpha)$ oscillates freely with evenly spaced nodes throughout the range $0 < \alpha < \frac{1}{2}\pi$; the nodes shift slowly away from $\alpha = \frac{1}{4}\pi$ as R increases. An essential difference here is that in Fig. 3(a) the amplitude at the antinode $\alpha = \frac{1}{4}\pi$ increases with R, while in Fig. 3(b) it decreases gradually with R near the node at $\alpha = \frac{1}{4}\pi$. In region (B), $g_\rho(R;\alpha)$ is confined to the potential ditches, the more narrowly the larger R. Here $g_\rho(R;\alpha)$ is essentially hydrogenic in accordance with Eq. (20a) and its variation with R is smooth, with $g_\rho(R;\alpha)$ peaking at smaller values of α (or of $\frac{1}{2}\pi - \alpha$) as R increases. In this region, Figs. 3(a) and 3(b) behave similarly; both reduce to hydrogenic $2s$ wave functions in the small-α region, with vanishing amplitude at $\alpha \sim \frac{1}{4}\pi$. One important difference in the plots of Figs. 3(a) and 3(b) is the way $g_\rho(R;\alpha)$ varies in passing from region (A) to region (B). In Fig. 3(b) this transition occurs smoothly and gradually, the amplitude near $\alpha \approx \frac{1}{4}\pi$ decreases progressively to zero in approaching region (B). However, the transition in Fig. 3(b) is different. One notices that the amplitudes $g_\rho(R;\frac{1}{4}\pi)$ increase with R in

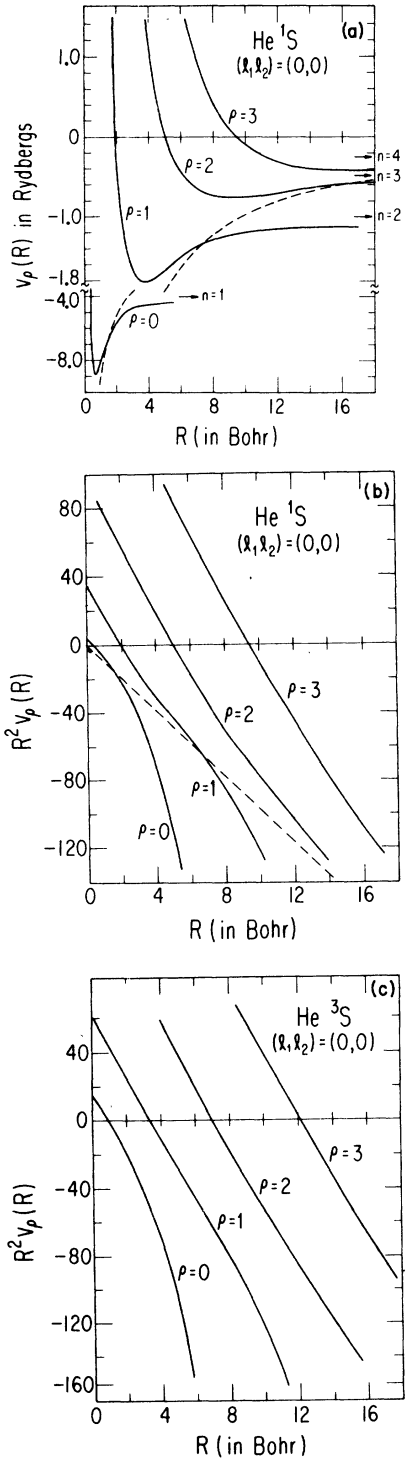

FIG. 2. (a) Solid line, potential curves $v_\rho^{(00)}(R)$ of helium ^1S channels converging to the $-4/n^2$ limits of He^+ at large R; dashed line, locus of avoided crossings between adjacent curves [Eq. (24)]. (b) Plots of $R^2v_\rho^{(00)}(R)$. (c) $R^2v_\rho^{(00)}(R)$ plots for helium ^3S. Absence of clearly avoided crossings in contrast with Fig. 2(b).

region (A) but decrease to zero in region (B). In the transition region (C), the amplitude at $\alpha=\frac{1}{4}\pi$ changes from a maximum value to nearly zero in a small interval of R; this behavior is associated with the "bumps" in the plots of $R^2v_\rho(R)$ observed at the avoided crossing in Fig. 2(b). On the other hand, the transition from region (A) to region (B) is smooth in Fig. 3(b) and this behavior is associated with the absence of bumps in the plots of $R^2v_\rho(R)$ in Fig. 2(c).

The fast variation of $g_\rho(R;\alpha)$ near $\alpha=\frac{1}{4}\pi$ in region (C) of Fig. 3(a) is not limited to the $\rho=1$ case only; in fact, it is a general property of all channel functions of ^1S states. The transition occurs when $v_\rho(R)$ is approximately equal to the potential energy in the flat region of the potential in Fig. 1, namely, when

$$v_\rho(R_c)\approx -C(\tfrac{1}{4}\pi,\pi)/R_c=-\sqrt{2}(4Z-1)/R_c\,. \qquad (22)$$

Dotted lines representing this equation in the figures confirm that it represents the locus of avoided crossings. For the ^3S states $\alpha=\frac{1}{4}\pi$ is a node at all R; the amplitude $g_\rho(R;\alpha)$ varies smoothly with R in the proximity of this node as we pass from region (A) to region (B).

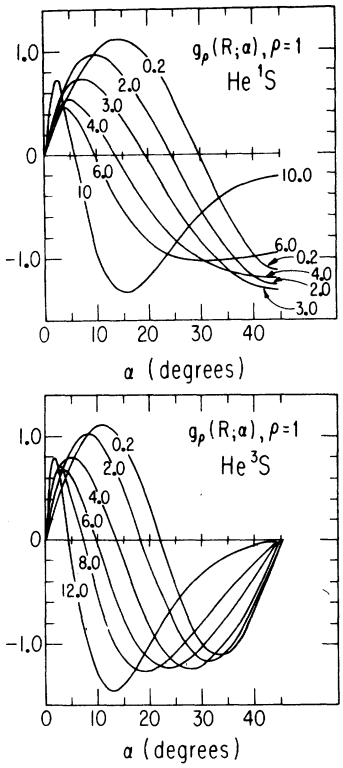

FIG. 3. (a) Channel functions $g_1^{(00)}(R;\alpha)$ for helium ^1S for $0\le\alpha\le\frac{1}{4}\pi$ and various R. The value of $g_1^{(00)}$ near $\alpha=\frac{1}{4}\pi$ peaks at $R=3$ and then decreases. (b) Same as (a) for ^3S.

Regions of avoided crossing are of critical importance to an understanding of the excitation mechanism, as we shall see in Sec. IV D, because the channel functions change most rapidly there. To get a closer look at these changes, we plot in Figs. 4(a) and 4(b) the equidensity lines of $g_\rho^2(R;\alpha)$ for $\rho=0$ and 1, respectively, in the polar coordinates $(R;\alpha)$; the two figures are very similar except for the presence of nodal lines in Fig. 4(b). Each figure shows a region (A) with large density along the $\alpha=\frac{1}{4}\pi$ line and another region (B) at larger R where this density has fallen sharply, peaking instead near $\alpha=0$ and $\frac{1}{2}\pi$. Examine particularly Fig. 4 in the range of R between 1.5 and 2.5 where Fig. 2(b) shows an avoided crossing between the channels $\rho=0$ and 1. This region coincides with the transition from region (A) to region (B) in Fig. 4(a), where the peaking of density at $\alpha=\frac{1}{4}\pi$ falls rapidly, but coincides in Fig. 4(b) with the *buildup toward* the peak density in region (A) for the $\rho=1$ channel. This behavior appears to be quite general: The *drop of the value of* $g_\rho^2(R;\alpha)$ *in one channel,* as it passes from region (A) to region (B) along $\alpha=\frac{1}{4}\pi$, occurs at the avoided crossing with channel $\rho+1$ and is accompanied by the *rise of* $g_{\rho+1}^2(R;\frac{1}{4}\pi)$ *in the next channel* toward the peak of its region (A). A transition from the lower channel to the next higher one at their avoided crossing would thus *preserve a density maximum along the* $\alpha=\frac{1}{4}\pi$ *line;* that is, it would preserve a high probability for the two electrons to be equidistant from the nucleus. The implications of this remark will be developed in Sec. IV D. For ^3S states, on the contrary, this behavior is totally absent, as $g_\rho(R;\alpha)$ remains small near its node at $\alpha=\frac{1}{4}\pi$.

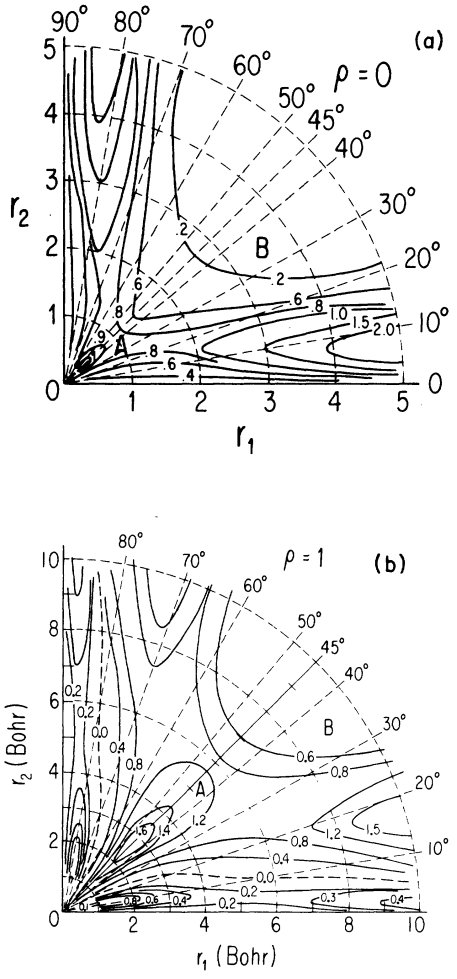

FIG. 4. Equidensity plots of $|g_\rho^{(00)}(R;\alpha)|^2$ of helium ^1S channels in the polar coordinates (R,α); (a) for $\rho=0$, (b) for $\rho=1$. Peak near $\alpha=45°$ (Region A) occurs at larger R in (b) than in (a). Nodal line at small α occurs only in (b).

C. Properties of $v_\rho^{(l_1l_2)}(R)$ and $\phi_\rho^{(l_1l_2)}(R;\Omega)$ with $l_1\neq l_2$; plus and minus channels

When $l_1\neq l_2$, the coordination scheme is complicated by the convergence of pairs of v_ρ to the same R limit, and the properties of $\phi_\rho(R;\Omega)$ are more difficult to analyze because of incomplete separability of radial, angular, and exchange correlations. However, the understanding obtained in Sec. IV B for S states will provide surprisingly useful guidance.

In Fig. 5, we show $R^2v_\rho(R)$ for helium $^1P^0$ states with $(l_1,l_2)=(1,0)$. Additional results for helium $^3P^0$ show similar features.[17] A remarkable novelty of these plots is that one can distinguish two groups of curves with the characteristic behaviors of ^1S and ^3S, respectively. The group analogous to ^1S curves of Fig. 2(b) corresponds to $\rho=0,1,3,5\ldots$, the other corresponds to $\rho=2,4,6,\ldots$, and is represented by dashed lines. This distinction is confirmed and illustrated by the plots of functions $g_\rho(R;\alpha)$—analogous to those of Eq. (21)—which is shown in Fig. 6. The group analogous to the ^1S shows an antinode near $\alpha=\frac{1}{4}\pi$, the other group shows a node in that region, though not exactly at $\alpha=\frac{1}{4}\pi$. This characterization on the basis of antinodes and nodes is just that pointed out in Ref. 4 as the earmark of plus and minus states.

After this brief initial reference to the functions g_ρ, we should explain that their meaning is not quite the same as in the case of $l_1=l_2$. The analog of Eq. (21) for $l_1\neq l_2$ is

$$\phi_\rho^{(l_1l_2)}=g_\rho^{(l_1l_2)}(R;\alpha)\mathcal{Y}_{l_1l_2LM}(\hat{r}_1,\hat{r}_2)+(-1)^{l_1+l_2-L+S}g_\rho^{(l_1l_2)}(R;\tfrac{1}{2}\pi-\alpha)\mathcal{Y}_{l_2l_1LM}(\hat{r}_1,\hat{r}_2). \tag{23}$$

The presence of two terms is required by exchange symmetrization, which was assured automatically in the case of $l_1 = l_2$ by the symmetry of each g_ρ. The superposition of two terms of Eq. (23) makes it more difficult to describe the electron correlations; we do not pursue this matter but confine ourselves here to analysis of the separate terms of Eq. (23). We have simplified this analysis further by removing from the matrix (16) the elements that couple $\mathcal{Y}_{l_1 l_2 LM}$ with $\mathcal{Y}_{l_2 l_1 LM}$ by exchange of orbital momentum, i.e., that couple the two terms of the channel function of Eq. (23). This has been done for the calculation of the function g_ρ shown in Fig. 6 for helium P states with $(l_1 l_2) = (1, 0)$ by disregarding the dipole component of electron-electron interaction. The elimination of this coupling term suppresses the difference between singlets and triplets, but has a qualitative effect only near the large-R limit, as will be discussed below.

We consider now why the plus and minus curves for ^1P states resemble the curves for ^1S and ^3S states, respectively, in order to anticipate whether this resemblance should occur generally for $l_1 \neq l_2$. One important feature in Fig. 6(b) is that the location of the node at $\alpha \approx 50^\circ$ hardly changes with R, in contrast to other nodes in Figs. 3 and 6 that shift progressively away from the midpoint. We have examined the $g_\rho(R; \alpha)$ plots for $\rho = 4$ and 6 also and have found that they also have a node near $\alpha = \frac{1}{4}\pi$ which does not change position with R. This nearly fixed node near $\alpha = \frac{1}{4}\pi$ corresponds to the node at $\alpha = \frac{1}{4}\pi$ for ^3S states whose location is fixed by antisymmetry. In both the minus channels and ^3S channels, the amplitude of $g_\rho(R; \alpha)$ near $\alpha = \frac{1}{4}\pi$ is small and decreases monotonically with R. On the other hand, the plus channel functions, like those of ^1S states, have an antinode near $\alpha = \frac{1}{4}\pi$ in region (A) where the oscillation of $g_\rho(R; \alpha)$ is nearly free. The existence of a node or antinode in $g_\rho(R; \alpha)$ near $\alpha = \frac{1}{4}\pi$ for each pair of plus and minus channels that converge to the same large-R limit can be understood by working backward from the large-R limit toward small R. In the large-R region, the hydrogenic states nl_1 and nl_2 are degenerate, each of them confined in one of the potential ditches of Fig. 1. As R decreases, their wave functions can penetrate into the $\alpha \approx \frac{1}{4}\pi$ region and overlap. This process is analogous to the introduction of a weak coupling between two oscillators whose frequencies need only be roughly equal; the coupling results in a plus mode characterized by an antinode at or near the midpoint and a minus mode characterized by a node in the same region. In our two-electron problem the "midpoint" $\alpha = \frac{1}{4}\pi$ represents configurations with the two electrons equidistant from the

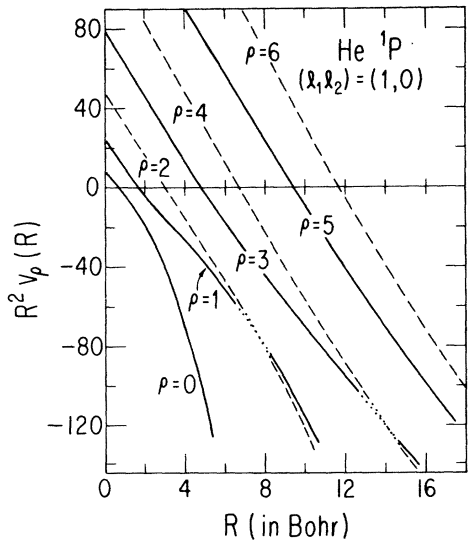

FIG. 5. $R^2 v_\rho^{(10)}$ for helium ^1P channels. Straight line, plus channels; dashed line, minus channels; dotted line, crossing treated diabatically (see text).

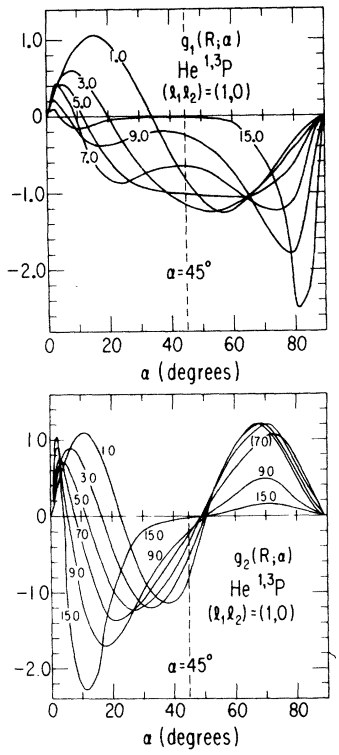

FIG. 6. Channel function component $g_\rho^{(10)}(R; \alpha)$ [Eq. (23)] for helium for $0 < \alpha < \frac{1}{2}\pi$ and various R; (a) $\rho = 1$, (b) $\rho = 2$. $g_1^{(10)}(R; 50^\circ)$ peaks at $R \sim 3$, while $g_2^{(10)}$ decreases monotonically near the node. These $g_\rho^{(10)}(R; \alpha)$ were obtained by neglecting the dipole component of the electron-electron interactions and thus are the same for ^1P and ^3P channels.

nucleus; the probability of these configurations approaches a relative maximum in plus modes, a relative minimum in minus modes. This analysis suggests strongly that the existence of pairs of channels with plus and minus characters is a general property of all $l_1 \neq l_2$ cases, provided only that pairs of channel eigenvalues $\upsilon_\rho^{(l_1 l_2)}$ are sufficiently close to degeneracy at large R.

The preceding analysis shows that the properties of $g_\rho(R;\alpha)$ in ^1S channels hold for the plus channels in the case of $l_1 \neq l_2$, whereas those of ^3S channels apply to the minus channels. In particular, the properties of regions (A), (B), and (C) of the mapping in Fig. 4 discussed in Sec. IV B for ^1S channels carry over to the plus channels. The existence of region (C) for plus channels but not for minus channels should explain that plus channels are more likely to be excited, as will be discussed further in Sec. IV D.

At large R, where the υ_ρ of each (+, −) pair are nearly degenerate, their separation depends mostly on the dipole interaction between the elements whose effect we had suppressed for purpose of analysis at lower R. This interaction affects the channel functions $g_\rho(R;\alpha)$ qualitatively, causing each of them to approach a superposition of $P_{nl_1} \times (R\sin\alpha)$ and $P_{nl_2}(R\sin\alpha)$. Since the importance of various correlation effects in determining the values of υ_ρ change with R, for each pair of (+, −) channels the transition of potential curves from lower R to the nearly degenerate larger-R region may suffer sudden variations if υ_ρ's are obtained by straightforward diagonalization of the matrix (16). Indeed, such sudden variations occur at a modest value of R for ^1P channels (at $R \approx 7.0$ between $\rho = 1.2$ and $R \approx 13.5$ between $\rho = 3, 4$), but only gradually at larger R for ^3P channels.[3,17] In Fig. 5 we have dotted in the section of υ_1 and υ_2 near the avoided crossing to stress that in this region it may be desirable to depart from the adiabatic procedure in the calculation of υ_ρ and $g_\rho(R;\alpha)$ in favor of a diabatic procedure that would allow υ_1 and υ_2 to cross, achieving a smoother variation of both the υ_ρ and the g_ρ.

D. Excitation mechanism and couplings between channels

We return now to the system of coupled equations (12), identifying its channels μ with the channels $(l_1 l_2 \rho)$ described in Secs. IV B and IV C. According to Eq. (12) the channels interact through two types of coupling, represented, respectively, by the off-diagonal terms of $\underline{U}$ and $\underline{W}$. The off-diagonal terms of $\underline{U}$ connect channels with different $(l_1 l_2)$ and will be discussed in Sec. V. In this section we will evaluate and discuss coupling terms $(l_1 l_2 \rho|\, W \,|\, l_1 l_2 \rho')$ in connection with the process of excitation from one channel to the other.

We regard the atomic excitation process as analogous to the molecular orbital theory of electron promotion[20] in ion-atom or atom-atom collisions. Transition from one electronic state to another is attributed to nonadiabatic transitions from the ground state to excited molecular orbitals during the collision process. Both ion-atom and electron-atom collisions start from large R in the energetically lowest channel ($\rho = 0$ in our case) with a constant angular momentum (LS in our case). Photoabsorption by an atom occurs instead in the low-R region occupied by the atom in its ground state, but it also brings the atom initially into a state of its $\rho = 0$ channel, because radial wave functions $F_\rho(R)$ with $\rho \neq 0$ are excluded from this region by the centrifugal barrier represented by large values of υ_ρ. In either case we must then solve the complete Schrödinger equation (12) for $\psi = \sum_\rho F_\rho(R)\phi_\rho \times (R;\Omega)$ with initial values of $F_\rho(R)$ that vanish for all $\rho \neq 0$. Transition to other channels, represented by the occurrence of nonzero values of F_ρ with $\rho \neq 0$, should result from the action of off-diagonal elements of $\underline{U}$ and $\underline{W}$ in the process of integration of Eq. (12). Upon completion of this integration the squared amplitude of outgoing wave components $F_\rho(R)$, with $\rho \neq 0$, at large R represents the probability of excitation in an electron-atom collision or of a double process of ionization-plus-excitation in the case of photoabsorption. In the process of integration the main contribution to transitions to $\rho \neq 0$ should occur where the coupling terms between the channels are largest. According to Eq. (13), this would be where $d\phi_\rho/dR$ is large, i.e., when ϕ_ρ varies rapidly in region (C) of Figs. 3 and 6.

From the results of Secs. IV B and IV C, we anticipate that *direct transition* from lower channels to higher channels should be *unlikely*. At small R, all higher channels are prevented from getting any significant amplitudes because of large centrifugal potentials at larger R, where the wave motions for lower channels are confined in the potential ditches of Fig. 1. In both cases, excitation to higher channels is unlikely. Therefore, transition from a $\rho = 0$ channel to high channels seems likely to occur *via intermediate channels*, i.e., through a sequence of nonadiabatic transitions in the avoided-crossing region between successive channels; these occur at higher and higher values of R. Thus, for (00ρ) channels of helium ^1S states, transition from the $\rho = 0$ channel to $\rho = 1$ should occur at $R \approx 1.5$ and the transition from $\rho = 0$ to $\rho = 2$ should occur via the $\rho = 1$ channel, through the avoided crossing between $\rho = 0$ and 1 at $R \approx 1.5$ and $\rho = 1$ and 2 at $R \approx 6$. Excitation to higher-ρ channels is described similarly, through the successive avoided crossings between adjacent channels at values of R given by

Eq. (22). This can also be anticipated from the behavior of channel functions obtained in Secs. IV B and IV C.

The above discussion emphasizes the excitations to higher channels based upon the occurrence of regions of avoided crossing between adjacent channels. It implies that channels without any well-developed region of avoided crossing [region (C) of Sec. IV B] should have smaller excitation cross sections; equivalently, the doubly excited states of such channels should have smaller decay widths. Indeed, the ^3S channels of Sec. IV B and the minus channels of Sec. IV C show no evidence of avoided crossing between the channels; accordingly the excitation cross sections for ^3S states should bear the same ratio to those for ^1S states as those for minus channels bear to plus channels. Existing evidence confirms this expectation. Experimentally the decay widths of the doubly excited states of helium ^1P states in the plus and minus channels are in the ratio of ~100:1. Close coupling and other calculations[21] for He** show that the decay widths for the $2sns$ ^1S states are also about 100 times larger than those of the $2sns$ ^3S states. For ^3P states, the decay widths for the plus and minus channels are also approximately in this ratio. The same holds for the electron-hydrogen excitation process. The excitation cross sections from $1s$ to $2s$ or $2p$ calculated by close-coupling methods[22] indicates that the contributions from ^1S and ^3S partial waves are in the ratio of ~100:1.

We proceed now to consider to what extent this seemingly consistent picture is borne out by analysis and evaluation of the channel coupling terms of Eq. (14). The influence of channel ρ' upon the equation for the radial wave function F_ρ of channel ρ is represented by the inhomogeneous term $W_{\rho\rho'}F_{\rho'} = 2(\phi_\rho, d\phi_{\rho'}/dR)\,dF_{\rho'}/dR + (\phi_\rho, d^2F_{\rho'}/dR^2)F_{\rho'}$. Existing data[17] on the matrix elements $(\phi_\rho, d\phi_{\rho'}/dR)$ and $(\phi_\rho, d\phi_{\rho'}/dR^2)$ do show that these coupling terms are rather small, as expected. Yet they are not sufficiently small to make it obvious that the channel coupling can be treated by perturbation methods and will, in fact, yield transition probabilities of the correct order of magnitude.

Numerical tests have been conducted to estimate the transition probabilities among ^1S and among ^1P channels. The result turns out to be too large by one-half order of magnitude. They also were found to depend on integrals over more than one wavelength of radial functions F_ρ and hence sensitive to the accuracy of these functions, all of which is also rather unexpected. These tests were conducted starting from channel functions Φ_μ obtained in Sec. V. We conclude tentatively at this time that an adiabatic channel basis Φ_μ does not provide the degree of decoupling of channels that we anticipated from the evidence reviewed in Sec. I and which seemed borne out by the striking properties of channel functions described in Secs. IV B and IV C. In other words, the properties of the adiabatic channels do not quite match those of the physical channels.

V. ADIABATIC POTENTIAL CURVES

In this section we indicate how the potential curves $v_\rho^{(l_1l_2)}$ are changed by electron-electron interactions involving transfer of angular momentum between the two electrons. We give examples for helium ^1S and ^1P states and for ^1S states of H^-. The calculation of energy levels and of decay widths for various L, S, π combinations will be the subject of later publications.

Interactions between different $v_\rho^{(l_1l_2)}$ are taken into account by completing the diagonalization of the matrix $\underline{U}$ of Eq. (17). The resulting adiabatic potential curves $U_\mu(R)$ should coincide with those of Ref. 3. The corresponding adiabatic channel functions are represented by

$$\Phi_\mu(R;\Omega) = \sum_{(l_1l_2\rho)} a^\mu_{l_1l_2\rho}(R)\phi_\rho^{(l_1l_2)}(R;\Omega)\,. \tag{24}$$

The mapping of these functions is complicated by nonseparability; at this state we can only discuss the correlations qualitatively on the basis of knowledge of the $\phi_\rho^{(l_1l_2)}$ and of the coefficients $a^\mu_{l_1l_2m}(R)$. The construction of $\underline{W}(R)$ on this new basis is described in Ref. 17.

Since the off-diagonal matrix elements of $\underline{U}$ [Eq. (17b)] are small, as explained in Sec. IV, they are important only when $v_\rho^{(l_1l_2)}$ for different $(l_1l_2\rho)$ channels are nearly degenerate. Therefore the coefficients $a^\mu_{l_1l_2\rho}$ for each value of μ will be significantly nonzero for a few sets of $(l_1l_2\rho)$ only. Often these sets will belong only to potential curves $v_\rho^{(l_1l_2)}$ that converge to the same large-R limit.

Figure 7 shows the three adiabatic potential curves of helium ^1P states that converge to the $n = 2$ limit of He^+. Also shown are $v_1^{(10)}$, $v_2^{(10)}$, and $v_0^{(21)}$ in dashed lines. We note that $\mu = 1$ curve lies very close to $v_1^{(10)}$, indicating weakness of the interactions that involve transfer of angular momentum between $(l_1, l_2) = (1, 0)$ and $(2, 1)$. Also we see that the $\mu = 2$ curve is not far from $v_2^{(10)}$ for $R > 4$; accordingly its channel function remains close to $\phi_2^{(10)}$ of the $s\rho$- channel. The crossing between $v_2^{(10)}$ and $v_0^{(21)}$ at $R \approx 4.2$ introduces, however, appreciable pd components in higher bound eigenstates of the $\mu = 2$ channel, whose energies approach the ordinate -1.1 Ryd in Fig. 7; this admixture has been noted before.[23] On the other hand, the potential curve of the pd channel is raised appreciably and thus its channel function ϕ_3 has appreciable

$\phi_2^{(10)}$ component.

We have also made a few pilot calculations for ^1S states of H^-. In the following we only mention some interesting characteristics peculiar to H^-. Among all the potential curves $v_\rho^{(l_1 l_2)}$ of the ^1S channel that converge to a given limit n of H, only the s^2 curve, with $(l_1 l_2) = (0, 0)$, shows a potential minimum below $-1/n^2$ limit while all others are *completely repulsive*. Figure 8(a) shows the two curves $v_1^{(00)}$ and $v_0^{(11)}$ in dashed lines, together with the two adiabatic potential curves U_1 and U_2. Here again U_1 has a well but U_2 is completely repulsive. Figure 8(b) shows the three adiabatic curves U_μ that converge to the $n = 3$ limit of H. The three $v_2^{(00)}$, $v_1^{(11)}$, and $v_0^{(22)}$ curves are not shown, but we know that only $v_2^{(00)}$ is attractive. Among the three $U_\mu(R)$, with $\mu = 3, 4, 5$, U_3 has a normal well, U_4 a shallow well and outer barrier, and U_5 is completely repulsive. The type of potential $U_4(R)$ has the effect of causing delayed, or "shape" resonances; such resonances have been discussed in other instances of electron-neutral atom collisions[24] near threshold but without any explicit reference to an effective potential. The height of the outer potential barrier in the $\mu = 4$ curve of Fig. 8(b) corresponds to an energy 12.13 eV above the ground state of H, which compares well with the shape resonance at 12.16 eV observed experimentally.[25]

VI. APPLICATION TO SPECTRA OF ALKALINE EARTH ATOMS

This section illustrates the potential application of our approach by examples pertaining to many-electron atoms. We connect some of the properties of Λ^2 operator discussed in Sec. II with strong correlation effects that have been observed in the spectra of alkaline earths, whose two optical electrons move outside a closed-shell ion core. As emphasized in preceding sections, correlation effects at small R are mainly determined by the kinetic-energy operator Λ^2. We also recall from Sec. II that electron-electron interactions involving transfer of angular momentum between two electrons are weak in general, but important in cases of degeneracy. Two unusually strong correlation effects will, in fact, be traced to such degeneracies.

(a) The first example occurs when the potential curves $v_\rho^{(l_1 l_2)}$ of different $(l_1 l_2)$ cross at small R. Crossing occurs for the ^1S channels that are designated by (001) and (110) in the $(l_1 l_2 \rho)$ notation of this paper and which contain $2\,sns$, $2\,pnp$ states, respectively. It also occurs for the ^1S channel which contain $3\,sns$, $3\,pnp$, and $3\,dnd$ states. As shown in Sec. IV, all the potential curves $v_\rho^{(l_1 l_2)}$ are given by $v_\rho \sim [(l_1 + l_2 + 2m + 2)^2 - R(l_1 l_2 m | C | l_1 l_2 m)]/R^2$, with $\rho = \frac{1}{2}m$ at small R. For $R \sim 0$, these values of v_ρ are ordered according to increasing values of $\nu = l_1 + l_2 + 2m = l_1 + l_2 + 4\rho$. Therefore, the curve $v_0^{(11)}$ starts below $v_1^{(00)}$ at $R \sim 0$, but since $(002|C|002)$ is larger than $(110|C|110)$, the two curves will cross at somewhat larger R. As discussed in

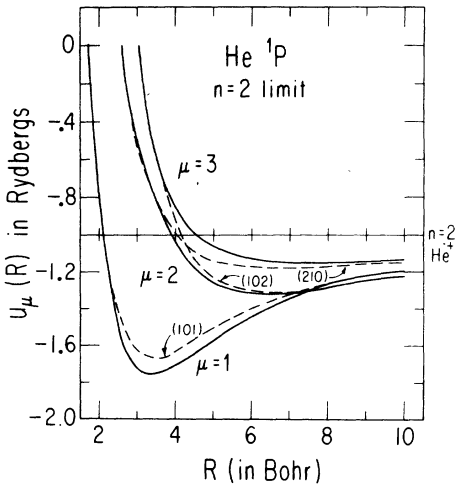

FIG. 7. Potentials for helium ^1P channels converging to the $n = 2$ limit of He^+. Straight line, U_1, U_2, and U_3; dashed line, $v_1^{(10)}$, $v_2^{(10)}$, and $v_0^{(21)}$.

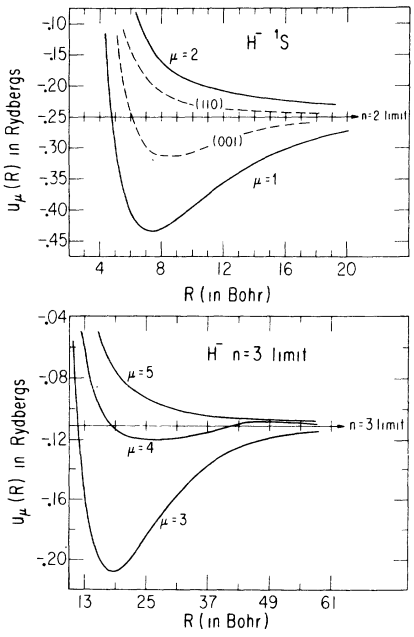

FIG. 8. (a) Potentials for H^- ^1S channels converging to the $n = 2$ limit of H. Straight line, U_1 and U_2; dashed line, $v_1^{(00)}$ and $v_0^{(11)}$. (b) Adiabatic potential curves U_3, U_4, and U_5 of H^- ^1S channels converging to the $n = 3$ limit of H.

Sec. V, the off-diagonal element $(001|U|110)$ caused then a considerable mixing of the two channel functions near the crossing which lies, at least in He, at values of R somewhat lower than the mean radius of the $2s^2$ state and much lower than the radius of the $2p^2\ ^1S$ state. This remark interprets the strong mixing of the $2s^2\ ^1S$ and $2p^2\ ^1S$ states of beryllium and possibly also of the $ns^2\ ^1S$ and $np^2\ ^1S$ of all other alkaline-earth atoms. Note also that the wave functions of $2\,sns\ ^1S$ states do not have appreciable amplitude at small R where the crossing occurs; accordingly, their admixture of $2p^2\ ^1S$ is weak, even though their energy levels lie closer to the $2p^2\ ^1S$ level than $2s^2\ ^1S$ does. The argument presented here has, of course, only indicative value, in the absence of calculations specifically designed for alkaline-earth atoms rather than for He.

(b) Strong correlation also occurs when two eigenfunctions of Λ^2 with the same LS quantum numbers are degenerate. For example, this degeneracy occurs normally at $R=0$ for ^1D channels with $(l_1, l_2)=(2,0)$ and with $(l_1, l_2)=(1,1)$ because they have equal values of l_1+l_2. In this case, the channel coupling due to electron-electron interaction remains important and produces appreciable mixing of channel functions over a large range of R. Thus it is not surprising that all $nsmd\ ^1D$ $(m>n)$ states of alkaline earths interact strongly with the $np^2\ ^1D$ state; in fact, the coupling does not decrease much with increasing m and extends into the continuum.[26] A closely related phenomenon of strong mixing occurs also in atoms with three valence electrons; here a strong admixture of $2snp^2\ ^2D$ is found throughout the $2s^2nd\ ^2D$ channel.[27] In fact, the degeneracy at $R=0$ considered here occurs rather generally for all values of $L \geq 2$.

ACKNOWLEDGMENTS

I wish to express my appreciation to Professor U. Fano for suggesting this problem, for his guidance throughout the work, and his help in the preparation of the manuscript. I also thank Professor J. H. Macek for discussions and advice.

---

*Work supported in part by the U.S. Atomic Energy Commission under Contract No. C00-1674-93, and in part by the Advanced Research Projects Agency.

†Presented to the Department of Physics, The University of Chicago, in partial fulfillment of the requirements for the Ph.D. degree.

‡Present address: Harvard College Observatory, 60 Garden Street, Cambridge, Mass. 02138.

[1]R. P. Madden and K. Codling, Phys. Rev. Lett. 10, 516 (1963); Astrophys. J. 141, 364 (1965).

[2]U. Fano, in *Atomic Physics*, edited by B. Benderson, V. W. Cohen, and F. M. Pichanick (Plenum, New York, 1969), Vol. I, p. 209.

[3]J. Macek, J. Phys. B 1, 831 (1968).

[4]J. W. Cooper, U. Fano, and F. Prats, Phys. Rev. Lett. 10, 518 (1963).

[5]C. E. Wulfman, Phys. Lett. 26A, 397 (1968).

[6]J. S. Alper and O. Sinanoğlu, Phys. Rev. 177, 77 (1969); J. S. Alper, Phys. Rev. 177, 86 (1969). See also A. R. P. Rau, Phys. Rev. A 2, 1600 (1970); J. S. Alper, Phys. Rev. A 2, 1603 (1970).

[7]O. Sinanoğlu and D. R. Herrick (unpublished).

[8]For triatomic molecular systems, see R. C. Whitten and F. T. Smith, J. Math. Phys. 9, 1103 (1968) and references therein; for the nuclear three-body problem see, e.g., W. Zickendraht, Ann. Phys. 35, 18 (1965).

[9]A. M. Ermolaev and G. B. Sochilin, Dokl. Akad. Nauk SSSR 155, 1050 (1963) [Sov. Phys.—Dokl. 9, 292 (1964)]; C. L. Pekeris, Phys. Rev. 146, 46 (1966).

[10]V. Fock, Kgl. Norske Videnskab. Selskab, Forh. 31, 145 (1958); R. J. White and F. H. Stillinger, J. Chem. Phys. 52, 5800 (1970).

[11]P. M. Morse and H. Feshbach, *Methods of Theoretical Physics* (McGraw-Hill, New York, 1953), p. 1755.

[12](a) D. L. Knirk, J. Chem. Phys. 60, 66 (1974); (b) J. Chem. Phys. 60, 760 (1974); (c) Phys. Rev. Lett. 32, 651 (1974).

[13]F. T. Smith, Phys. Rev. 120, 1058 (1960).

[14]J. H. Macek, Phys. Rev. 160, 170 (1967).

[15]G. Breit, Phys. Rev. 35, 569 (1930); A. K. Bhatia and A. Temkin, Rev. Mod. Phys. 36, 1050 (1964). See also Ref. 11, pp. 1720–28.

[16]When θ_{12} is one of the angular coordinates, the symmetrization of the wave function is not represented by a general formula but must be treated separately for each L, S, π. For two-electron problems, see Ref. 15; for the nuclear three-body problems, see Zickendraht, Ref. 8.

[17]C. D. Lin (unpublished).

[18]U. Fano and C. D. Lin, The Fourth International Conference on Atomic Physics, Heidelberg, July, 1974 (to be published).

[19]F. T. Smith, Phys. Rev. 179, 111 (1969).

[20]U. Fano and W. Lichten, Phys. Rev. Lett. 14, 627 (1965); W. Lichten, Phys. Rev. 164, 131 (1967); M. Barat and W. Lichten, Phys. Rev. A 6, 211 (1972).

[21]See, for example, the literature cited in Ref. 3.

[22]P. G. Burke, S. Ormonde, and W. Whitaker, Proc. Phys. Soc. Lond. 92, 319 (1967).

[23]K. T. Chung and I. H. Chen, Phys. Rev. Lett. 28, 783 (1972).

[24]P. G. Burke and A. J. Taylor, J. Phys. B 2, 869 (1969); D. L. Moores and D. W. Norcross, J. Phys. B 5, 1482 (1972).

[25]G. J. Schulz, Rev. Mod. Phys. 45, 378 (1973). In particular, see Fig. 9.

[26]K. T. Lu, J. Opt. Soc. Am. 64, 44 (1974).

[27]C. D. Lin, Astrophys. J. 187, 385 (1974); A. W. Weiss, Phys. Rev. A 9, 1524 (1974).